Cosmic Noise Absorption Observed with Imaging Riometer in Alaska: Use of CNA to Estimate Energy Spectra of Auroral Precipitating Electrons

TANAKA Yoshimasa, ISHII Mamoru, KUBOTA Minoru, MURAYAMA Yasuhiro, MORI Hirotaka, and Dirk Lummerzheim

Since the NICT's 256-element imaging riometer was installed at Poker Flat, Alaska, in 1995 in cooperation with the Geophysical Institute of the University of Alaska Fairbanks, it has been recording the high-spatial-resolution cosmic noise absorption (CNA) to study the effect of high-energy electron precipitation on the polar middle atmosphere. We examined how to use the CNA data to estimate the energy distribution of auroral precipitating electrons. In this paper, we describe the method to extract the information of the flux of high-energy precipitating electrons by combining CNA with the optical emissions observed at two wavelengths with the all-sky imager.

Keywords
Imaging riometer, All-sky imager, Cosmic noise absorption, Auroral precipitating electrons, Energy distribution

1 Introduction

Recent years have seen growing interest among the international community regarding global-scale environmental issues such as global warming and holes in the ozone layer. It is important to note that essential to understanding the true nature of the problems we face in this respect is the resolution of the basic causal link between solar activity and global environmental changes. In particular, we must look at the polar regions: these areas experience an efficient influx of energy from solar winds and auroras, and it is believed that the dynamics and the chemical processes of the upper polar atmosphere are strongly influenced by these phenomena. For example, the equivalent power consumption associated with a single aurora event is estimated to reach up to 1 billion kW, and the Joule heating induced by such an event in turn heats the atmosphere. However, studies aimed at investigating the quantitative effects of auroras on neutral atmosphere have yet to progress to any significant degree.

Stationary observations of auroras are mainly carried out using ground-based remote-sensing techniques. To date, the popular method for estimating the energy of auroral precipitating electrons from the ground consisted of determining the intensity ratio of monochromatic auroral luminosity for two wavelengths[1]. This method is based on certain known relationships: the altitudes of auroral emissions, and the types of molecules or ions that are excited, which are dependent on the energies of the precipitating electrons. This method, which makes use of auroral

light, is suitable for estimating precipitating electron energies in the range of several hundred eV to several keV.

Electrons having higher energies (above 10 keV) penetrate into the ionospheric D region at altitudes less than 100 km and induce ionization and heating of the atmosphere in the region. An increase in electron density in the ionospheric D region has been known to cause absorption of cosmic radio noise, a phenomena referred to as cosmic noise absorption (CNA). Therefore, through CNA observations, it is possible to obtain information on high-energy electron precipitation accompanying an auroral event. In order to perform stationary CNA observation with high spatial resolution, NICT has developed a 256-element imaging riometer, installed at Poker Flat, Alaska, USA in 1995[2]. Figure 1 shows the main beam pattern of the 256-element imaging riometer. The field of view of the present instrument at an altitude of 90 km is 400 km × 400 km, and the spatial resolution is approximately 7˚(11 km) near the zenith. The images are taken at a rate of one per second during 24-hour continuous observation.

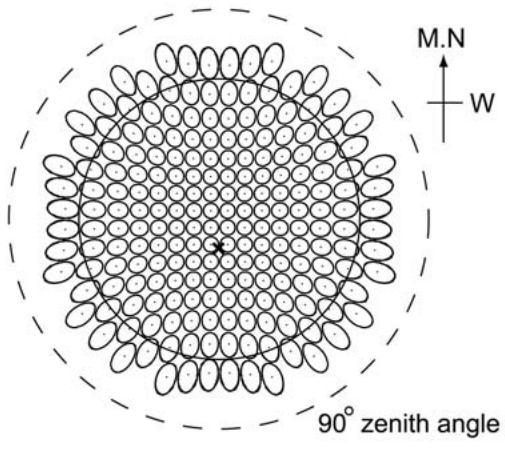

Fig.1 *The −3 dB contour lines of the main beam of the 256-element imaging riometer (polar coordinate plot)*

The outer (dashed line) and inner (solid line) circles correspond to the 90˚ and 60˚ zenith angles, respectively. The cross near the center of the circle indicates the direction of the magnetic zenith.

Although the CNA acquires data on high-energy electrons of 10 keV or greater, few studies so far have attempted to perform energy distribution estimations by combining CNA results with optical observation data. One reason that this combination has yet to be performed can be seen in the inferior spatial resolution of the riometer compared to optical observations, which complicates comparison of riometer data against optical observation results of aurora with small-scale structures. Another factor is seen in significant uncertainties in atmospheric parameters at CNA altitudes that prevented any quantitative discussion. Thus, in the present paper, we will test a method for obtaining an energy distribution that makes use of high-spatial-resolution CNA data observed using the imaging riometer in combination with auroral monochromatic luminosity data, followed by a discussion of the various potential applications of the method.

2 Method of analysis

In the present method of analysis, emissions and CNA are compared by converting the respective physical quantities into comparable forms. Following is a description of the relevant analytical procedures. (1) The characteristic energy and total energy flux of the incident electrons are calculated using the dual-wavelength monochromatic auroral emission data, assuming that the energy distribution of the incident electron follows the Maxwellian distribution. (2) CNA is calculated using the obtained incident electron energy distribution as input, and the result is compared with the observed CNA. The details of the analytical process are presented below.

2.1 Estimation of precipitating electron energy based on monochromatic auroral emission

The present analysis employs the two wavelengths for N_2^+ first negative band (wavelength: 427.8 nm) and O permitted line emission (wavelength: 844.6 nm). This analysis

requires model calculations of the auroral emission intensity; here, the appropriate calculations were made by adopting the one-dimensional electron transport equation[3]. It is assumed that the energy distribution of the incident electrons follows the Maxwellian distribution and that the pitch angle distribution follows an isotropic distribution. The incident altitude was set at 500 km. In this case, the differential directional number flux I(E) of the incident electrons is given by the following equation.

$$I(E) = \frac{Q_0}{2\pi E_c^3} E \exp\left(-\frac{E}{E_c}\right) \quad (1)$$

Here, E is energy, E_c is characteristic energy, and Q_0 is the total energy flux. The neutral atmospheric parameters were calculated according to the Mass Spectrometer, Incoherent Scatter Radar Extended Model 90 atmospheric model (MSIS 90 model)[4]. The MSIS 90 model requires input data such as the date, coordinates of the observation point, Ap index, F 10.7 index, etc., and appropriate values were selected according to observation conditions.

Figure 2 shows an example of the neutral atmospheric parameters used in analysis, such as the number density of the major molecular species, neutral atmosphere temperature, and the effective recombination coefficient for 9 UT on March 6, 2003. Figure 3 shows the dependence of volume emission rate on characteristic energy for the emissions of 427.8 nm and 844.6 nm calculated assuming a unit energy flux (1 mWm^{-2}) of incident electrons. It may be seen from this figure that the emission at 844.6 nm is effectively induced by electrons having lower energies compared to the 427.8-nm emission. The auroral emission intensity observed on the ground can be obtained by integrating the emission rate along the magnetic field line.

Figure 4 presents the characteristic-energy dependence of (a) intensity of the 427.8-nm line and (b) intensity ratio of the 844.6-nm line to the 427.8-nm line when assuming a unit energy flux (1 mWm^{-2}) of incident electrons. In the E_c range of 100 eV to 20 keV, the 427.8-nm line intensity is nearly constant regardless of characteristic energy, and it can be seen that the intensity ratio of the 844.6-nm line to 427.8-nm line decreases monotonously with increasing characteristic energy. These plots were fitted with appropriate functions to create a conversion equation between auroral emission intensity and characteristic energy. Using this equation, the characteristic energy and total energy flux were calculated from the

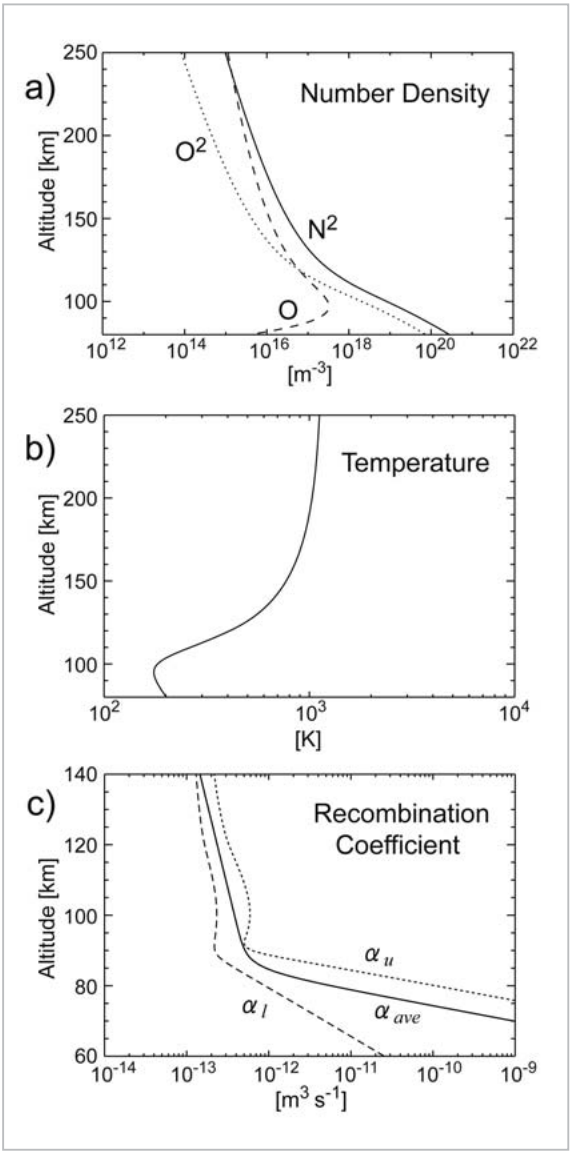

Fig.2 *Neutral atmospheric parameters for 9 UT on March 6, 2003*

(a) Molecular number density, (b) temperature of the neutral atmosphere, and (c) effective recombination coefficient

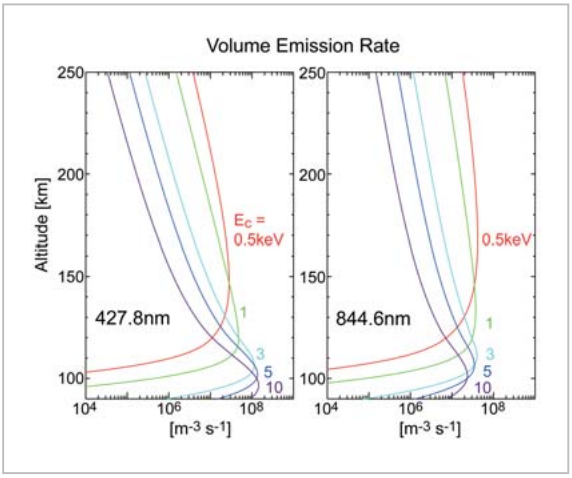

Fig.3 *Volume emission rate of aurora*

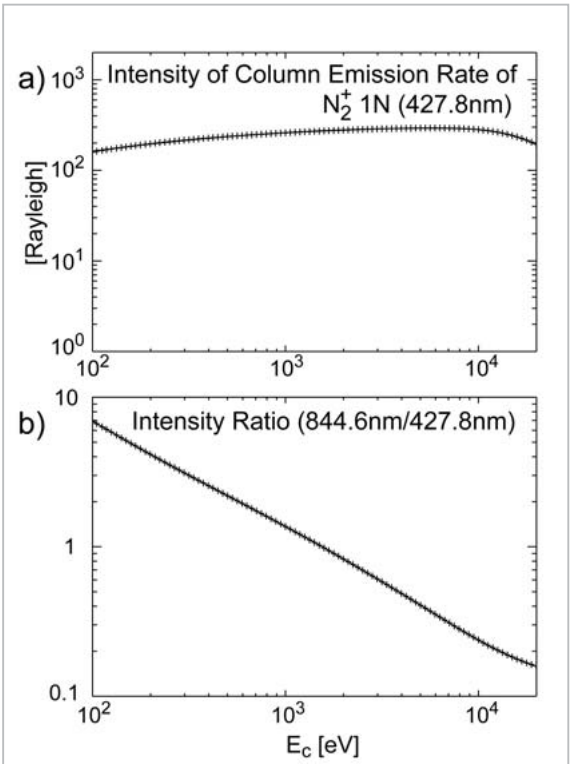

Fig.4 *Relationship between auroral emission intensity and characteristic energy*

(a) The intensity of 427.8-nm emission and (b) intensity ratio of 844.6-nm emission to 427.8-nm emission observed on the ground, calculated from incident electron of unit energy flux (1 mWm^{-2})

observed intensities of the 844.6-nm and 427.8-nm emissions.

2.2 Estimation of CNA

CNA is calculated using the incident electron flux obtained in Section **2.1**, using the following equation.

$$CNA_M = 4.6\times10^{-5}\int \frac{\nu(z)N_e(z)}{\omega^2+\nu(z)^2}dz. \qquad (2)$$

Here, CNA_M refers to the CNA estimated from optical observation data assuming that the incident electron energy distribution follows the Maxwellian distribution, and is represented in units of dB. In Eq. (2), the MKS unit system is used. $N_e(z)$ and $\nu(z)$ are electron density and electron-neutral collision frequency at altitude z, respectively. ω is the observation frequency (38.2 MHz). Figure 5a presents the vertical profile of $\nu(z)$ at 9 UT on March 6, 2003[5].

If temporal variations of electron density are assumed to be negligible, then $N_e(z)$ in Eq. (2) may be calculated using the following equation.

$$N_e(z) = \sqrt{\frac{\varepsilon(z)}{\Delta\varepsilon_{ion}\alpha(z)}} \qquad (3)$$

Here, $\varepsilon(z)$ is the energy deposition rate of incident electrons, $\Delta\varepsilon_{ion}$ is the average energy loss per ion pair production, and $\alpha(z)$ is the effective recombination coefficient. It was assumed here that $\Delta\varepsilon_{ion}$ is 35 eV for all molecules.

The $\varepsilon(z)$ in Eq. (3) was determined according to the range calculation method of Jackman et al. (1980), using the incident electron flux calculated in Section **2.1** as input[6][7]. Energy dissipation and range of high-energy electrons that penetrate into the ionospheric D region have been taken from Berger and Seltzer (1972)[8]. When auroral emission intensity is calculated using the transport equation in Section **2.1**, the electron density $N_e(z)$ is also obtained. However, such calculations are not applicable to the high-energy electrons that induce CNA.

The statistical average of the recombination coefficient during auroral events on the night side (α_{ave}), such as that shown in Fig. 2c, was used as the recombination coefficient

$\alpha(z)$[9]. The recombination coefficient is the parameter with the highest uncertainty in the present calculations, and this value has been known to display significant variations depending on season, local time, and electron density. In order to evaluate the ambiguity resulting from this uncertainty in the recombination coefficient, calculations were performed for two additional recombination coefficients (α_u and α_l). Here, α_u is a recombination coefficient arrived at by combining the recombination coefficient of NO^+ ($z > 90$ km)[10] with α_{ave} shifted in the positive direction ($z < 90$ km), at an altitude of 90 km. The value α_l is the recombination coefficient arrived at by combining the recombination coefficient of O_2^+ ($z > 90$ km)[10] with the average coefficient on the day side ($z < 90$ km), at around 90 km. These profiles of α_u and α_l reflect that NO^+ and O_2^+ are the major ion species at altitudes of 90–150 km, as well as the wide range of fluctuations in the recombination coefficient below 90 km, due to the effects of cluster ions and negative ions. The values for α_u and α_l below 90 km may be extreme values, and so the range of recombination coefficient values contained in the region sandwiched by these two curves nearly covers all values raised in discussions of past studies[11].

Figures 5b and 5c present the vertical profiles of $N_e(z)$ and CNA_M per unit altitude, respectively, calculated assuming a characteristic energy of 10 keV and total energy flux of 1 mWm^{-2} for incident electrons. As is clear from these figures, CNA_M occurs in a relatively thin layer at approximately 80–110 km.

A comparison was made between the CNA_M and the CNA actually observed using an imaging riometer ($\equiv CNA_{OBS}$). Here, we defined the difference between CNA_{OBS} and CNA_M ($CNA_{OBS} - CNA_M$) as δCNA. This value may be used as an indicator to judge the deviation of the high-energy band of precipitating electron flux from the Maxwellian distribution. In order to match the conditions of CNA_{OBS} and CNA_M, CNA_{OBS} was averaged over an exposure time for the all-sky imager. Since the exposure time for the optical data used in the present study was 45 seconds, the results of analysis presented in the next section are averaged images for a 45-second period. Moreover, the CNA_M was averaged within the −3 dB contours of the main lobe shown in Fig. 1. This calculation assumes that the auroral emission and CNA intensity is uniform within this range, that the main lobe is extremely narrow, and that the effects of the sidelobe are small. In order to perform a more rigorous analysis, it will be necessary to take

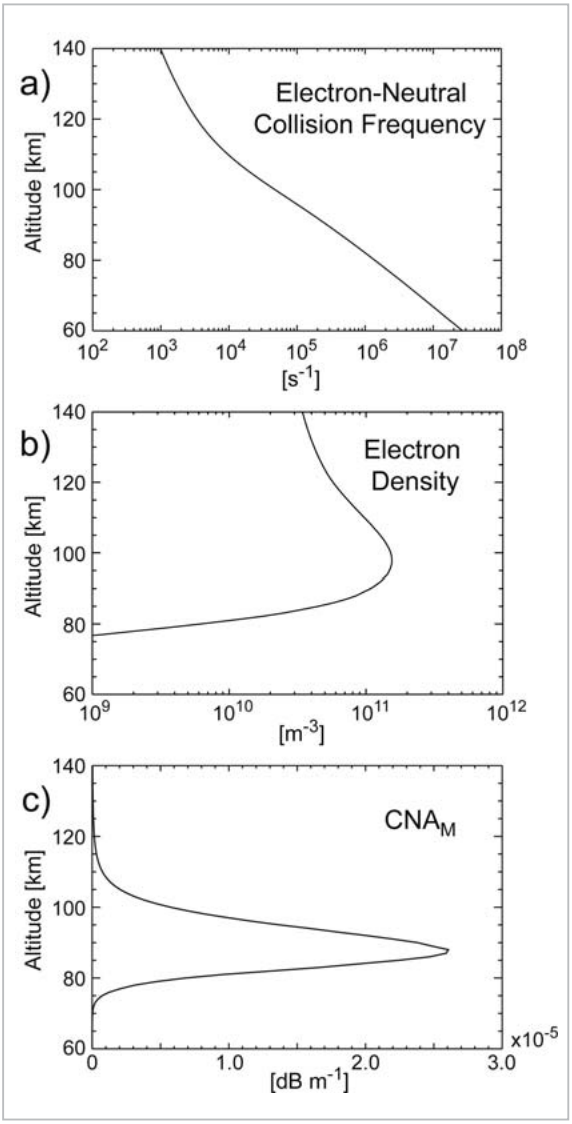

Fig.5 *Vertical profiles of electron-neutral collision frequency, electron density, and CNA*

(a) Electron-neutral collision frequency; (b) electron density and (c) CNA per unit altitude created by incident electron of E_c = 10 keV and Q_0 = 1 mWm^{-2}

antenna directivity into consideration, including the sidelobe.

3 Example of analysis for 10–14 UT on March 6, 2003

This section presents an example of analysis for the period 10–14 UT on March 6, 2003. The K_p index at the time was 4^- to 4^+, and geomagnetic activity was rather high. Figure 6 shows, from top to bottom: the magnetic NS (H) component; and, in the magnetic zenith direction, auroral emission intensity (427.8 and 844.6 nm), characteristic energy (E_c), total energy flux (Q_0), CNA_M, CNA_{OBS}, and δCNA. The values of these quantities in the magnetic zenith direction were defined as the average for two beams near the magnetic zenith measured with the imaging riometer. The CNA_M and δCNA calculated using α_u and α_l are also shown. It can be seen from these plots that the rapid decrease in the magnetic northward component (maximum of ΔH = approx. –1,300 nT) and the rapid increase in auroral emission are initiated by the explosive phase of a relatively large substorm that began at around 11:35 UT.

One of the prominent features in the temporal variation of δCNA is observed during the recovery phase of the 12:30–13:00 UT substorm. During this period, δCNA displays a gradual increase in the positive direction for all a values. This increase can be interpreted as a sign that the high-energy electron precipitation was heavier than had been predicted by the Maxwellian distribution. On the other hand, during the rapid increase in auroral emission and CNA_M at around 10:40 UT, δCNA takes a negative value, since only a slight increase was seen in the CNA_{OBS}.

Figures 7 and 8 show two-dimensional data for 12:37:05–12:37:50 UT (vertical line # 2 in Fig. 6) and 10:40:23–10:41:08 UT (vertical line # 1 in Fig. 6), respectively. Here, CNA_M and δCNA were calculated using the average recombination coefficient α_{ave}. In all panels, the zenith angle in the field of view is 60°, and the top and left coincide with the geographic north and east, respectively. It can be confirmed from Fig. 7 that a diffuse aurora covers a wide area of the sky during 12:37:05–12:37:50 UT, and that in most areas of the aurora, δCNA takes a positive value (green-red) due to the fact that $CNA_M < CNA_{OBS}$.

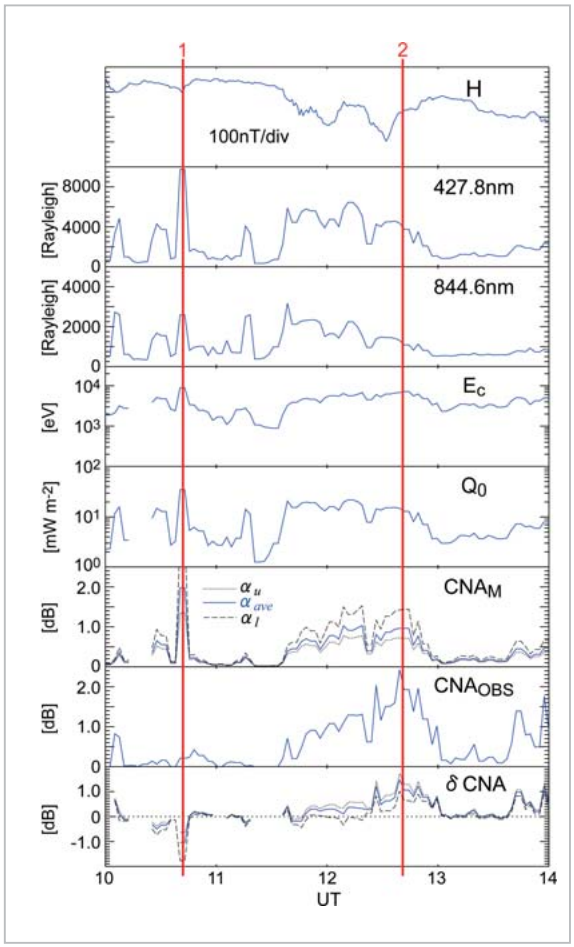

Fig.6 *Example of analysis for 10:00–14:00 UT on March 6, 2003*

The presence of a bright discrete auroral arc near the magnetic zenith can be confirmed in Fig. 8. Since it is obvious that $CNA_M > CNA_{OBS}$ and $\delta CNA < 0$ inside the arc, it may be conjectured that the energy distribution of the electrons precipitating along this arc reflects a far smaller high-energy electron flux compared to that predicted by the Maxwellian distribution.

The relationship between auroral types and signs of δCNA may be explained by the relationship between auroras observed by satellites and rockets, as well as by precipitating

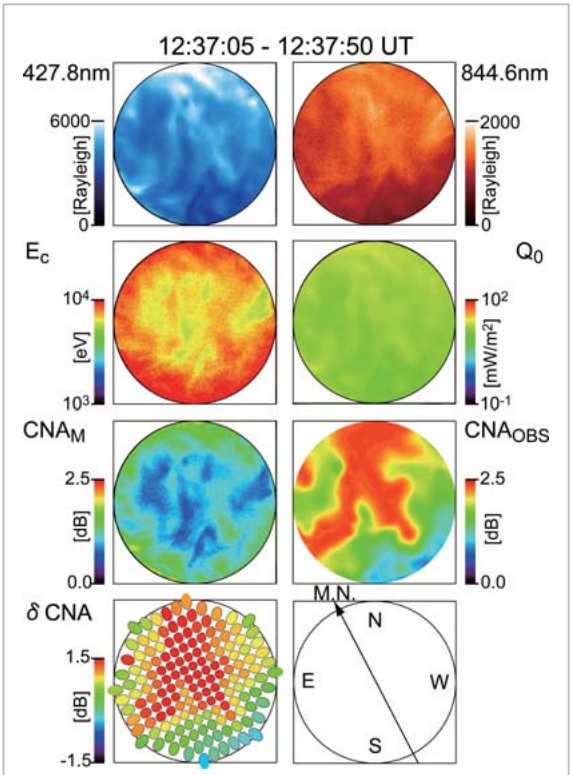

Fig.7 *Example of analysis for 12:37:05–12:37:50 UT, March 6, 2003 (2-D plot)*

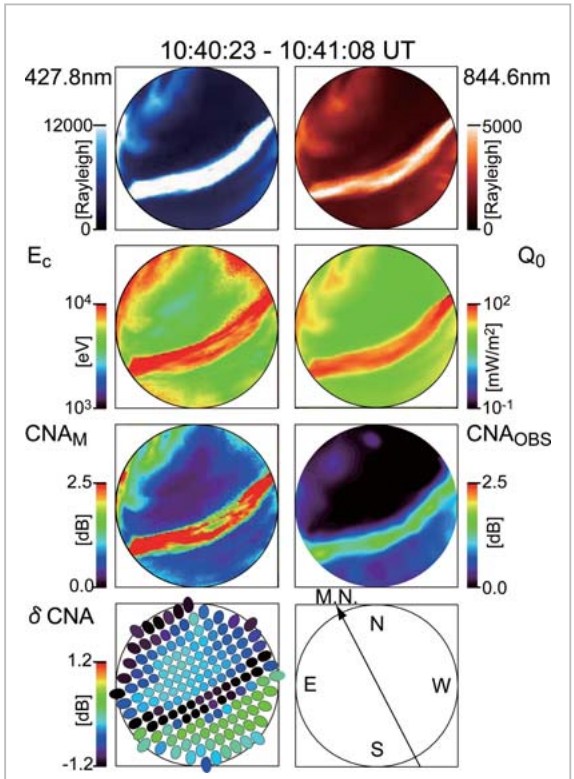

Fig.8 *Example of analysis for 10:40:23–10:41:08 UT, March 6, 2003 (2-D plot)*

electron energy distributions presented in past studies. For example, the distribution of electron precipitation accompanying discrete auroras generally displays a sharp peak in the energy band from a few hundred eV to a few keV, which is indicative of acceleration along the magnetic field line at altitudes of several thousands of kilometers from the ground[12]. The assumption that the energy distribution of such electron precipitation follows a Maxwellian distribution results in the overestimation of electron flux in the high-energy band relative to actual conditions (in other words, δCNA < 0). In contrast, it is believed that the precipitation of electrons that induce emission in the diffuse aurora during the substorm recovery phase is caused by pitch-angle scattering of electrons in the plasma sheet of the magnetosphere. Therefore, these emission-inducing electrons often display energy distributions that stretch toward the high-energy bands, as represented by the κ distribution (in other words, δCNA > 0)[12]. Thus it may be concluded that the δCNA obtained through the present analysis may prove useful to a certain degree in the estimation of the shape of the energy distribution.

In the regions of large zenith angles in Figs. 7 and 8 (the peripheral areas in the field of view), large values of E_c and CNA_M are observed. The appearance of these values may be caused by the wide altitudinal distribution of auroras, and by the different vertical emission profiles for different wavelengths.

4 Conclusions

In the present study, we tested a method of using CNA data in the estimation of auroral precipitating electron energy distribution. Information on the shape of the electron energy distribution was successfully obtained by calculating CNA based on auroral emission and comparing the results with the CNA observed with an imaging riometer. The 256-element imaging riometer installed at Poker

Flat, Alaska can generate beams that are much narrower than those of conventional riometers, which enables the acquired images to be compared with the results of optical observations of auroras having small-scale structures. Further, quantitative discussions on electron energy distributions should now be possible, through estimation of the ambiguities in the CNA resulting from uncertainties involving atmospheric parameters. The effectiveness of the present method of estimating energy distribution is supported to a certain degree by the consistency of the results obtained under this method with those obtained through past rocket and satellite observations.

In future studies, the validity of the energy distributions obtained by the present method must be examined against the results of direct observations using satellite. Moreover, in order to make more effective use of the high-spatial-resolution CNA data, it will also be necessary to develop more precise energy estimation methods for directions other than toward the magnetic zenith — such as a method for energy distribution estimation that takes into consideration the auroral vertical profile, as in auroral tomography.

Acknowledgements

The success of long-term stationary imaging riometer observations is attributable to the efforts of Jim Desrochers of the Geophysical Institute of the University of Alaska Fairbanks and the staff at the Poker Flat Research Range. We are deeply grateful to them all.

References

1 M. H. Rees and D. Luckey, "Auroral electron energy derived from radio of spectroscopic emissions 1. model computations", J. Geophys. Res., 79, 5181-5186, 1974.

2 Y. Murayama, H. Mori, S. Kainuma, M. Ishii, I. Nishimuta, K. Igarashi, H. Yamagishi, and M. Nishino, "Development of a high-resolution imaging riometer for the middle and upper atmosphere observation program at Poker Flat, Alaska", J. Atmos. Terr. Phys., 59, 925-937, 1997.

3 D. Lummerzheim, "Electron transport and optical emissions in the aurora", Ph.D. Thesis, University of Alaska, Fairbanks, 1987.

4 A. E. Hedin, "Extension of the MSIS thermosphere model into the middle and lower atmosphere", J. Geophys. Res.,96, 1159-1172, 1991.

5 K. M. Aggarwal, N. Nath, and C. S. G. K. Setty, "Collision frequency and transport properties of electrons in the ionosphere", Planet. Space Sci., 27, 753-768, 1979.

6 C. H. Jackman, J. E. Frederick, and R. S. Stolarski, "Production of odd nitrogen in the stratosphere and mesosphere: An intercomparison of source strengths", J. Geophys. Res.,85, 7495-7505, 1980.

7 D. Lummerzheim, "Comparison of energy dissipation functions for high energy auroral electron and ion precipitation", Geophysical Institute Report, UAG-R-318, University of Alaska, Fairbanks, 1992.

8 Berger and Sltzer, "Bremsstrahlung in the atmosphere", J. Atmos. Terr. Phys., 34, 85, 1972.

9 J. A. Gledhill, "The effective recombination coefficient of electrons in the ionosphere between 50 and 150 km", Radio Sci.,21, 3, 399-408, 1986.

10 M. H. Rees, "Physics and chemistry of the upper atmosphere", Cambridge university press, Cambridge, U.K., pp. 279-280, 1989.

11 J. M. Penman, J. K. Hargreaves, and C. E. McIlwain, "The relation between 10 to 80 keV electron precipitation observed at geosynchronous orbit and auroral radio absorption observed with riometers", Planet. Space Sci., 27, 445-451, 1979.

12 D. W. Swift, "Mechanisms for auroral precipitation: a review", Rev. Geophys. Space Phys., 19, 185-211, 1981.

***TANAKA Yoshimasa**, Dr. Sci.*

Project Reseacher, Transdisciplinary Research Integration Center, Research Organization of Information and Systems

Upper Atmospheric Physics

***KUBOTA Minoru**, Dr. Sci.*

National Institute of Information and Communications Technology

Dynamics in the Ionosphere and Thermosphere

***MURAYAMA Yasuhiro**, Dr. Eng.*

Planning Manager, Strategic Planning Office, Strategic Planning Department

Dynamics in the Thermosphere and Mesosphere

***Dirk Lummerzheim**, Ph.D.*

Research Professor, Geophysical Institute, University of Alaska Fairbanks

Auroral Physics

***ISHII Mamoru**, Dr. Sci.*

Research Manager, Space Environment Group, Applied Electromagnetic Research Center

Dynamics in the Ionosphere and Thermosphere

MONZEN Yoshizumi

Science Teacher, Yokohama Asahi Junior High School

Dynamics in the Ionosphere and Thermosphere

***MORI Hirotaka**, Dr. Sci.*

Key Technology Research Supporting Group, Key Technology Research Promotion

Upper Atmosphere Dynamics